Quantum Monte Carlo Algorithms for the Quantum Cluster Problem

M. Jarrell, A. Macridin and K. Mikelsons

Department of Physics, University of Cincinnati, Cincinnati, Ohio 45221

Abstract. We present a pedagogical discussion of the the Hirsch-Fye and Continuous time Quantum Monte Carlo (QMC) algorithms which may be used to study a correlated cluster embedded in an uncorrelated host, or used to solve the cluster problem in dynamical mean field theory (DMFT) or its cluster extensions. The basic algorithms are discussed, together with methods for efficient measurments and the modifications required by the self-consistency of the DMFT.

PACS: 02.70.Ss, 02.60.Pn, 71.27.+a

1. INTRODUCTION

The Hirsch-Fye and Continuous time Quantum Monte Carlo (QMC) algorithms are powerful and adaptable methods which may be used to study models of impurity clusters embedded in a host. As such, they are ideal cluster solvers for the embedded impurity problem at the heart of the Dynamical Mean Field and Dynamical Cluster Approximations.

In this chapter, we will illustrate to different QMC methods using Hubbard model Hamiltonian [1] as an example

$$H = H_0 + H_1 \tag{1}$$

with

$$\begin{aligned} H_0 &= -t \sum_{\langle j,k\rangle\sigma} (c^\dagger_{j\sigma} c_{k\sigma} + c^\dagger_{k\sigma} c_{j\sigma}) + \sum_j \varepsilon (n_{j\uparrow} + n_{j\downarrow}) \\ H_1 &= U \sum_j n_{j\uparrow} n_{j\downarrow}\,, \end{aligned} \tag{2}$$

where $c^\dagger_{j\sigma}$ ($c_{j\sigma}$) creates (destroys) an electron at site j with spin σ, $n_{i\sigma} = c^\dagger_{i\sigma} c_{i\sigma}$, and t sets a unit of energy.

We will sketch the Hirsch-Fye QMC in Sec. 2 and the weak coupling continuous time QMC algorithm in Sec. 3. Since both methods can be considered as expansions about the free electron limit, Wick's theorem applies to both, so similar methods for making and conditioning measurements described in Sec. 4 can be used for both HFQMC and CTQMC.

2. HIRSCH-FYE QMC

To derive the Hirsch-Fye algorithm, we start with the Hamiltonian

$$H = H_0 + H_1, \tag{3}$$

where H_0 is a noninteracting Hamiltonian and H_1 describes the interaction on a cluster (or impurity). Our derivation of the equations follows the one presented by Hirsch and

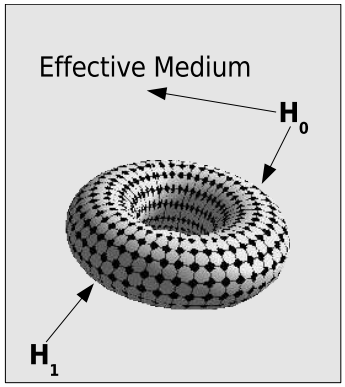

FIGURE 1. Hamiltonian breakup for the Hirsch-Fye derivation. H_0 describes both the host and non-interacting degrees of freedom of the cluster (impurity), while H_1 describes the interactions on the cluster.

Fye for the impurity problem [2, 3], but we extend the derivation to cluster embedded problems [4]. Let's assume for now that the interaction on the cluster is local

$$H_1 = U \sum_{i \in \mathscr{C}} (n_{i\uparrow} - \frac{1}{2})(n_{i\downarrow} - \frac{1}{2}) \, . \tag{4}$$

The summation in Eq. 4 is taken over the cluster, $\mathscr{C}$, sites.

By dividing the imaginary time (the inverse of the temperature) $\beta = \frac{1}{T}$ into L slices,

$$\Delta\tau = \frac{\beta}{L} \, , \tag{5}$$

the partition function can be written as

$$Z = Tr(e^{-\beta H}) = Tr\left(\prod_{l=1}^{L} e^{-\Delta\tau H}\right) \, . \tag{6}$$

From the Suzuki-Trotter formula

$$e^{-\Delta\tau H} = e^{-\Delta\tau H_0/2} e^{-\Delta\tau H_1} e^{-\Delta\tau H_0/2} + \mathscr{O}(\Delta\tau^3) \, , \tag{7}$$

one derives

$$Z = Tr(e^{-\beta H}) \approx Tr\left(\prod_{l=1}^{L} e^{-\Delta\tau H_0/2} e^{-\Delta\tau H_1} e^{-\Delta\tau H_0/2}\right) \tag{8}$$

which has leading errors proportional to $\Delta\tau^2$ (since the Suzuki-Trotter formula was applied L times and $L \sim 1/\Delta\tau$). Then due to the periodic property of the trace, it is easy to see that this is the same as the Trotter decomposition

$$Z = Tr(e^{-\beta H}) \approx Tr\left(\prod_{l=1}^{L} e^{-\Delta\tau H_0} e^{-\Delta\tau H_1}\right) \tag{9}$$

with leading errors still proportional to $\Delta\tau^2$.

We introduce the identity operator in the occupation number basis

$$I = \sum_m |m\rangle\langle m| \tag{10}$$

between exponents of operators at adjacent imaginary time slices. The partition function becomes

$$\begin{aligned} Z = \quad & \textstyle\sum_{m_L, m_{L-1}, .. m_1} \langle m_L | e^{-\Delta\tau H_0} e^{-\Delta\tau H_1} | m_{L-1}\rangle \langle m_{L-1} | e^{-\Delta\tau H_0} e^{-\Delta\tau H_1} | m_{L-2}\rangle \\ & \ldots \langle m_1 | e^{-\Delta\tau H_0} e^{-\Delta\tau H_1} | m_L\rangle \end{aligned} \tag{11}$$

With the identity due to Hirsch [5]

$$e^{-\Delta\tau U\left(n_{i\uparrow} n_{i\downarrow} - \frac{1}{2}(n_{i\uparrow} + n_{i\downarrow})\right)} = \frac{1}{2} \sum_{s_i = \pm 1} e^{\alpha s_i (n_{i\uparrow} - n_{i\downarrow})} , \tag{12}$$

with

$$\cosh \alpha = e^{\Delta\tau U/2} . \tag{13}$$

it is possible to introduce an auxiliary binary (± 1) field (called Hirsch-Hubbard-Stratonovich field, or HHS field) at every cluster site and at every time point. Thereby, the interacting problem described by Eq. 11 is replaced by a summation over all possible auxiliary field configurations of noninteracting terms. Eq. 12 can be proven by applying both the left and right hand sides on the four possible vectors (empty site, one electron up, one electron down and double occupied site) which span the local Hilbert space.

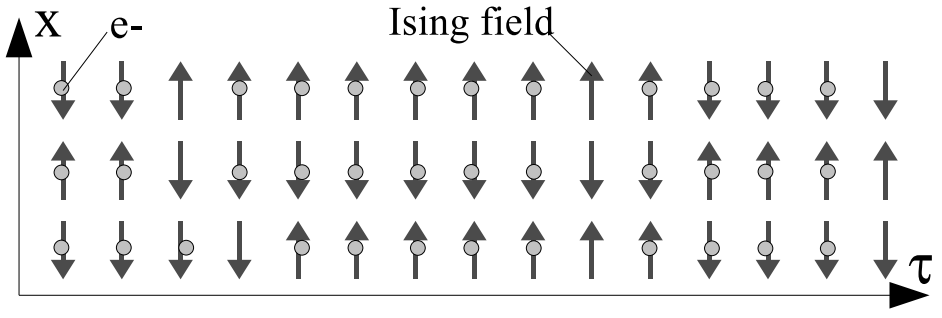

FIGURE 2. The Hirsch-Hubbard-Stratonovich transformation Eq. 12 maps an interacting systems of electrons onto a system of non-interacting electrons interacting with a time and space dependent Ising-like fields which coupling to the z-component of the electron spin.

For each HHS field configuration $\{s\}$, we have a noninteracting problem composed of electrons scattering off a space and time dependent Ising-like field (c.f. Fig. 2). Therefore, by defining

$$O_\sigma(s) = \begin{pmatrix} I & 0 & 0 & \dots & e^{-\Delta\tau K} e^{V_\sigma^L(s)} \\ e^{-\Delta\tau K} e^{V_\sigma^1(s)} & I & 0 & \dots & 0 \\ 0 & e^{-\Delta\tau K} e^{V_\sigma^2(s)} & I & 0 & \dots \\ \dots & & & & \\ \dots & \dots & \dots & e^{-\Delta\tau K} e^{V_\sigma^{L-1}(s)} & I \end{pmatrix} , \quad (14)$$

with

$$H_0 = \sum_{i,j,\sigma} c_{i\sigma}^\dagger K_{ij} c_{j\sigma} \quad (15)$$

and

$$V_\sigma^l(s)_{ij} = \begin{cases} \alpha\sigma s_{il}\delta_{i,j} & i \in \mathscr{C} \\ 0 & i \notin \mathscr{C} \end{cases} , \quad (16)$$

where s_{il} represents the value of HHS field at site i and time l, it is possible to write Eq. 11 as

$$Z = Tr_{\{s\}} \left[\det O_\uparrow(s) \ \det O_\downarrow(s) \right] \quad (17)$$

Note that every matrix element shown in Eq. 14 is in fact a $N \times N$ sub-block, N being the dimension of the K matrix defined in Eq. 15. Thus O is a $(N \times L) \times (N \times L)$ matrix.

The matrix O is the inverse of the one-particle Green's function

$$G_\sigma^{-1}(s) = O_\sigma(s) \ . \quad (18)$$

By defining

$$T_{il;jl'} = \delta_{l-1,l'}\delta_{i,j} \quad (19)$$

and

$$V_\sigma^l(s)_{il;jl'} = \begin{cases} \alpha\sigma s_{il}\delta_{l,l'}\delta_{i,j} & i \in \mathscr{C} \\ 0 & i \notin \mathscr{C} \ or \ j \notin \mathscr{C} \end{cases} , \quad (20)$$

Eqs. 14 and 18 can be written as

$$G_\sigma^{-1} = I - Te^{-\Delta\tau K} e^{V_\sigma} \ . \quad (21)$$

In Eq. 21 and in the following equations we omit writing the explicit HHS dependence for simplicity reasons. By multiplying Eq. 21 at right with e^{-V_σ} (which is diagonal) the following equation is obtained

$$G_\sigma^{-1} e^{-V_\sigma} = e^{-V_\sigma} - Te^{-\Delta\tau K}. \quad (22)$$

Eq. 22 is used to establish a relation between the Green's functions G' and G which correspond to two different field configurations $\{s\}$ and respectively $\{s'\}$

$$G_\sigma'^{-1} e^{-V_\sigma'} - G_\sigma^{-1} e^{-V_\sigma} = e^{-V_\sigma'} - e^{-V_\sigma} \ . \quad (23)$$

Using

$$A^{-1} - B^{-1} = C \Longleftrightarrow A = B - BCA \ , \tag{24}$$

the following equation is obtained

$$e^{V'_\sigma} G'_\sigma = e^{V_\sigma} G_\sigma + e^{V_\sigma} G_\sigma (e^{-V_\sigma} - e^{-V'_\sigma}) e^{V'_\sigma} G'_\sigma \tag{25}$$

After some easy manipulations, Eq. 25 can be written as

$$G'_\sigma = G_\sigma + (G_\sigma - I)(e^{V'_\sigma - V_\sigma} - I) G'_\sigma \ . \tag{26}$$

Another useful equation is

$$G_\sigma G'^{-1}_\sigma = I - (G_\sigma - I)(e^{V'_\sigma - V_\sigma} - I) \ , \tag{27}$$

obtained by multiplying Eq. 26 at right with G'^{-1}_σ. Eq. 27 will be used in the QMC process for calculating the transition probability form one configuration to another and Eq. 26 for updating to the new configuration when the transition is accepted.

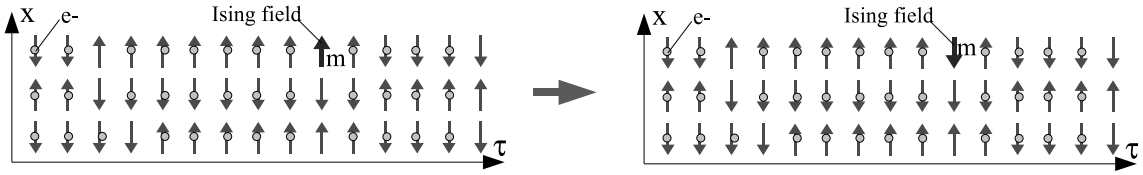

FIGURE 3. The original Hirsch-Fye algorithm involved local flips of the HHS fields.

The QMC algorithm implies generating different field configurations with a probability proportional to their weight, given by (see Eq. 17)

$$W(s) = \det G^{-1}_\uparrow(s) \det G^{-1}_\downarrow(s). \tag{28}$$

In the QMC process, the HHS field configuration is updated by proposing local (in both the cluster site and time index) flips of the HHS field (Fig. 3). We consider such two configurations (s and s') that differ only by a flip at point m, where m denotes both a cluster site and a time (i.e. $m \equiv il, i \in \mathscr{C}$). The ratio between the weights of these configurations is

$$R = \frac{W(s')}{W(s)} = \frac{\det G^{-1}_\uparrow(s') \det G^{-1}_\downarrow(s')}{\det G^{-1}_\uparrow(s) \det G^{-1}_\downarrow(s)}. \tag{29}$$

The ratio R determines the acceptance probability of the new configuration, according to either the Metropolis or the heat bath rule. If the proposed configuration was accepted, the new Green's function should be updated accordingly to Eq. 26. This implies the following

$$G'_{pn} = G_{pn} + (G_{pm} - \delta_{pm})(e^{\sigma\alpha(s'_m - s_m)} - 1) G'_{mn} \tag{30}$$

$$G'_{mn} = G_{mn} + (G_{mm} - 1)(e^{\sigma\alpha(s'_m - s_m)} - 1) G'_{mn} \tag{31}$$

$$G'_{mn} = \frac{G_{mn}}{1 - (G_{mm} - 1)(e^{\sigma\alpha(s'_m - s_m)} - 1)} \quad , \tag{32}$$

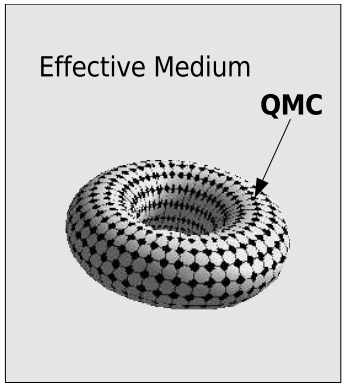

FIGURE 4. Whereas the HF Hamiltonian has degrees of freedom on the cluster and in the effective medium, the algorithm may be restricted to interacting (cluster) sites only.

which results in

$$G'_{pn} = G_{pn} + \frac{(G_{pm} - \delta_{pm})(e^{\sigma\alpha(s'_m - s_m)} - 1)}{1 - (G_{mm} - 1)(e^{\sigma\alpha(s'_m - s_m)} - 1)} G_{mn} \quad . \tag{33}$$

$$R = \frac{W(s')}{W(s)} = \prod_\sigma \det G'^{-1}_\sigma(s') \det G_\sigma(s) = \prod_\sigma [1 - (G_{\sigma mm} - 1)(e^{\sigma\alpha(s'_m - s_m)} - 1)]. \tag{34}$$

Eq. 34 results directly from Eq. 27. Note that only the Green's function defined between clusters sites is required for the QMC procedure. This is also enough for measuring the cluster observables and for determining the irreducible quantities as self-energy, Σ, and two-particle vertices, Γ's.

In order to initialize the QMC process, first the HHS fields are set to zero and G_σ is set to $\mathscr{G}_\sigma$. Here, $\mathscr{G}_\sigma$ is the noninteracting Green's function (i.e. the one obtained when $U = 0$) if we mean to simulate a finite size cluster, or its the cluster excluded Green's function (i.e. the one obtained when we subtract the self energy from the cluster) if we mean to simulate an embedded cluster. Afterwards, by turn, the value of HHS field is changed to 1 or -1 at all space-time points and the Green's function is updated in accordance to Eq. 33. The obtained Green's function is used to initialize the QMC procedure. A "sweep" of the QMC procedure consists of proposing a flip of the HHS field for every time slice, calculating (Eq. 34) the ratio R between the weights of the proposed and the present configuration and accepting the flip according to the Metropolis or the heat-bath algorithm. After a certain number of warm-up sweeps through the space-time points (usually between twenty and one hundred), the system reaches equilibrium and the measurements can start. It is a good idea to consider a few update sweeps between the measurements, in order to eliminate the correlation between them.

Numerical round-off errors accumulate in the Green's function during the updating process, e.g. Eq. 33. In order to eliminate them, after a certain number of iterations the Green's function should be refreshed. This is done first by setting G_σ to $\mathscr{G}_\sigma$ and afterwards updating it (using Eq. 33) to the corresponding HHS field.

2.1. Combining HFQMC with Quantum Cluster Methods

The Hirsch-Fye algorithm naturally produces Green's functions in Matsubara (imaginary) time. However, the self-consistency cycle of quantum cluster methods like the DMFA and DCA require imaginary frequency Green's functions. Thus the algorithm requires Fourier transforms from both the imaginary frequency to the imaginary time and from the imaginary time to the imaginary frequency. The transform from frequency to time is given by

$$G(\tau) = \frac{1}{\beta} \sum_{n=-\infty}^{\infty} G(i\omega_n)\, e^{-i\omega_n \tau} \tag{35}$$

and the inverse one, from time to frequency, by

$$G(i\omega_n) = \int_0^\beta d\tau\, G(\tau)\, e^{i\omega_n \tau} \ . \tag{36}$$

The Matsubara frequencies for the fermionic Green's function are defined as

$$\omega_n = \frac{(2n+1)\pi}{\beta} \ . \tag{37}$$

Due to the finite $\Delta\tau$, the numerical implementation of these transformations requires special care. We will discuss both cases next.

Transform from frequency to time. In Eq. 35 the frequency summation is taken from minus to plus infinity. The contribution at large (both positive and negative) frequency is important, thus a truncation of the sum is not possible. The trick is to subtract and add back a function which has at large frequency the same asymptotic behavior as the Green's function. For example, if $f(i\omega_n)$ fulfills this condition, Eq. 35 can be approximated by

$$G(\tau) \approx \frac{1}{\beta} \sum_{n=-n_c}^{n_c} (G(i\omega_n) - f(i\omega_n)) e^{-i\omega_n \tau} + \frac{1}{\beta} \sum_{n=-\infty}^{\infty} f(i\omega_n)\, e^{-i\omega_n \tau} \ , \tag{38}$$

where n_c is a cutoff number chosen large enough to have negligible numerical errors.

In order to determine the Green's function behavior at large frequency we integrate Eq. 36 by parts

$$\begin{aligned} G(i\omega_n) &= \tfrac{1}{i\omega_n} G(\tau) e^{i\omega_n \tau} \,|_0^\beta - \tfrac{1}{i\omega_n} \textstyle\int_0^\beta G'(\tau) e^{i\omega_n \tau} d\tau = \\ &= \tfrac{1}{i\omega_n} G(\tau) e^{i\omega_n \tau} \,|_0^\beta - \tfrac{1}{(i\omega_n)^2} G'(\tau) e^{i\omega_n \tau} \,|_0^\beta + \mathcal{O}((i\omega_n)^{-3}) \ . \end{aligned} \tag{39}$$

We find that, for cutoff values of about ≈ 500, it is necessary to consider the asymptotic behavior of G up to second order in ω_n^{-1}. If only the first order term in ω_n^{-1} is considered, in order to get negligible numerical errors the cutoff number n_c should be of order 10^6. Thus, the second order term in Eq. 39 has a major practical importance and therefore $f(i\omega_n)$ should be taken as

$$f(i\omega_n) = \frac{a_1}{i\omega_n} + \frac{a_2}{(i\omega_n)^2} \tag{40}$$

with

$$a_1 = -G(\beta^-) - G(0^+) = G(0^-) - G(0^+) \tag{41}$$

and

$$a_2 = G'(\beta^-) + G'(0^+) = -G'(0^-) + G'(0^+) \; . \tag{42}$$

The last sum in Eq. 38 can be easily calculated by using the following relations

$$\frac{1}{\beta} \sum_{n=-\infty}^{\infty} \frac{e^{-i\omega_n \tau}}{i\omega_n} = \begin{cases} \frac{1}{2} & \tau < 0 \\ -\frac{1}{2} & \tau > 0 \end{cases} \tag{43}$$

and

$$\frac{1}{\beta} \sum_{n=-\infty}^{\infty} \frac{e^{-i\omega_n \tau}}{(i\omega_n)^2} = \begin{cases} -\frac{1}{4}(\beta + 2\tau) & \tau < 0 \\ -\frac{1}{4}(\beta - 2\tau) & \tau > 0 \end{cases} \; . \tag{44}$$

The first of these relations (Eq. 43) is the well known Fourier transform of a noninteracting Green's function [6]

$$\frac{1}{\beta} \sum_{n=-\infty}^{\infty} \frac{e^{-i\omega_n \tau}}{i\omega_n - E} = \begin{cases} \frac{1}{e^{\beta E}+1} e^{-E\tau} & \tau < 0 \\ -(1 - \frac{1}{e^{\beta E}+1}) e^{-E\tau} & \tau > 0 \end{cases} \; . \tag{45}$$

with the energy pole $E = 0$. Eq. 44 results from differentiating Eq. 45 with respect to E and setting $E = 0$ afterwards.

The coefficients a_1 and a_2 in Eq. 40 can also be easily determined. Starting with the Green's function definition

$$G_{ij}(\tau) = -T_\tau \langle c_j(\tau) c_i^\dagger \rangle \; , \tag{46}$$

where i and j are space or momentum indices and using Eq. 41, a_1 becomes

$$a_1 = \langle c_i^\dagger c_j \rangle + \langle c_j c_i^\dagger \rangle = \delta_{ij} \; . \tag{47}$$

Considering

$$\frac{dc_j}{d\tau} = [H, c_j] \tag{48}$$

the coefficient a_2 is

$$a_2 = -\langle c_i^\dagger [H, c_j] \rangle - \langle [H, c_j] c_i^\dagger \rangle \; , \tag{49}$$

and can be evaluated to

$$a_2 = K_{ij} + K_{ij}^{HF} \; . \tag{50}$$

K_{ij} was defined in Eq. 15 and represent the bilinear (noninteracting) part of the Hamiltonian. K_{ij}^{HF} results from the interacting part of the Hamiltonian when the corresponding Hartree-Fock factorization is done.

Transform from time to frequency.. The difficulties associated with this transform are related with the fact that in the QMC process the Green's function is calculated and stored only in a discrete set of points τ_i evenly spaced by $\Delta\tau$. This implies a periodic Fourier transform with the period equal to the Nyquist critical frequency

$$\omega_c = \frac{\pi}{\Delta\tau} , \tag{51}$$

which is evidently unphysical, since the Green's function goes as ω_n^{-1} at large frequency (see Eq. 39). Besides that, due to the fact that part of the spectral density at high frequency ($\mid \omega \mid > \omega_c$) is translated into the low frequency domain ($\mid \omega \mid < \omega_c$), a phenomenon called *aliasing* [7], the Fourier transform is inaccurate even at frequencies smaller than the Nyquist frequency.

In order to cure [8] the pathology discussed above we again take advantage of our knowledge of the Green's function behavior at high frequency. A function which has the right large frequency asymptotic behavior is the Green's function G_p obtained from second order perturbation theory (or any other method which becomes exact at high frequency). The Fourier transform can be written as

$$G(i\omega_n) = G_p(i\omega_n) + \int_0^\beta d\tau (G(\tau) - G_p(\tau)) e^{i\omega_n \tau} . \tag{52}$$

It is important that the last term in Eq. 52 does not produce spurious high frequency contributions. Therefore before integration the Akima spline [9] is used to interpolate $G(\tau) - G_p(\tau)$. The Akima spline produces smooth curves and therefore acts as a low-pass filter and eliminates the high frequency noise.

3. CONTINUOUS TIME QUANTUM MONTE CARLO

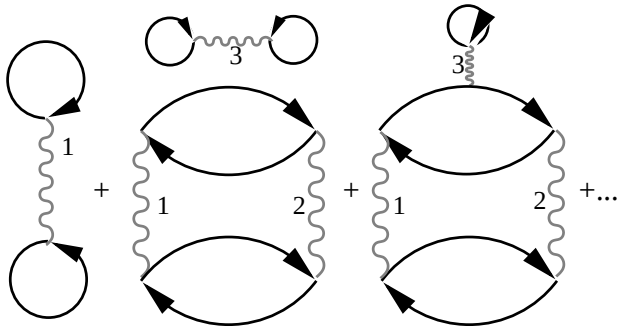

FIGURE 5. In contrast to HFQMC which employs a path-integral formalism, CTQMC uses QMC to stochastically sample the graphs in the partition function.

In this subsection, we will derive a Continuous time QMC (CTQMC) algorithm for the Hubbard model, Eq. 2 following closely the derivation by Rubtsov [10]. In contrast to the path integral formalism of HFQMC, CTQMC employs the same tricks used to derive Feynman-Dyson perturbation theory (the interaction representation, the time-ordered

S-matrix expansion, Wick's theorem, etc.) to stochastically generate diagrams for the partition function.

Starting with

$$\exp\left(-\beta(H_0+H_1)\right) = \exp\left(-\beta H_0\right) S(\beta) \tag{53}$$

where

$$S(\beta) = T_\tau \exp\left(-\int_0^\beta H_1(\tau) d\tau\right) \tag{54}$$

where T_τ is the time-ordering operator, and

$$H_1(\tau) = e^{\tau H_0} H_1 e^{-\tau H_0} \tag{55}$$

is the quartic part of H in the interaction picture.

Specializing now on the Hubbard model, Eq. 2, the partition function becomes

$$Z = Z_0 \sum_k \frac{(-U)^k}{k!} \int \cdots \int d1 \cdots dk \qquad \left\langle T_\tau n_\uparrow(1) \cdots n_\uparrow(k) \right\rangle_0 \left\langle T_\tau n_\downarrow(1) \cdots n_\downarrow(k) \right\rangle_0 \tag{56}$$

where $1 \rightarrow (x_1, \tau_1)$, etc. and $\langle\rangle_0$ indicates a thermodynamic average with respect to $\exp(-\beta H_0)$. Since H_0 is noninteracting, we can apply the Wick's theorem to evaluate the expectation values in Eq. 56 (see, for instance, [6]), by evaluating and summing over all closed Feynman graphs, see for example Fig. 6. For each order in k, there are $k!$ graphs

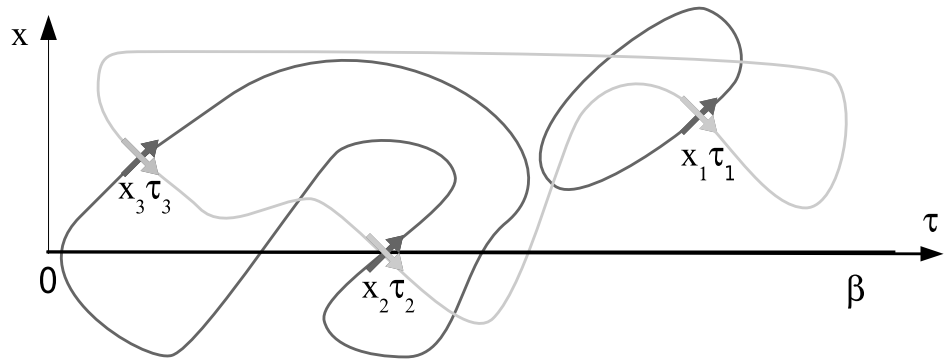

FIGURE 6. An example of a third-order ($k = 3$) CTQMC graph. Many graphs may be drawn to third order in U, one example is shown.

that can be drawn for each of the up and down electrons. Note that the graphs can include both connected and disconnected parts, as shown in the figure. According to Wick's theorem, each graph corresponds to a product of non-interacting Green's functions G^0 (i.e. Green's functions from the solution of H_0 only) with arguments determined by the vertex labels, etc., and sign determined by the number of line crossings. For example, the graph shown is

$$G^0(2,3)G^0(3,2)G^0(1,1)G^0(3,2)G^0(2,1)G^0(1,3) \tag{57}$$

where G^0 with the same argument are to be interpreted as having the right time argument slightly greater. I.e. $G^0(1,1) = G^0(x_1\tau_1; x_1\tau_1+)$. There will be 36 such graphs for each

$k = 3$ vertex configuration, and the number of graphs will increase with order like $k!$[2]. Fortunately, we may conveniently represent them as the product of up and down determinants $\det D_\uparrow(k) \det D_\downarrow(k)$, where

$$D_\sigma(k) = \begin{pmatrix} G^0_\sigma(1,1) & G^0_\sigma(1,2) & \cdots & G^0_\sigma(1,k) \\ G^0_\sigma(2,1) & G^0_\sigma(2,2) & \cdots & G^0_\sigma(2,k) \\ G^0_\sigma(3,1) & G^0_\sigma(3,2) & \cdots & G^0_\sigma(3,k) \\ . & . & . & \\ . & . & . & . \\ . & . & . & . \\ G^0_\sigma(k,1) & G^0_\sigma(k,2) & \cdots & G^0_\sigma(k,k) \end{pmatrix} \tag{58}$$

where, in lieu of an external field the bare Green's function does not need a spin label, $G^0_\sigma(k,2) = G^0(k,2)$. Note that $D_\sigma(k)$ is a $k \times k$ matrix.

In CTQMC, the sum of integrals in the Eq. 56 is evaluated using an importance sampling Monte Carlo algorithm. Suppose the cluster has N sites and $L = \beta/\Delta\tau$ time locations (in the end we may let $\Delta\tau \to 0$). We will consider Monte Carlo moves of adding vertices at a random location in space-time or subtracting existing vertices. By combining such moves, we can clearly access all possible vertex configurations. Consider two configurations, one with k and the other with $k+1$ vertices, then the weights W of these two configurations are given by the integrand of Eq. 56, or, in terms of the $D_\sigma(k)$,

$$\begin{aligned} W_k &= (-\Delta\tau U)^k \det D_\uparrow(k) \det D_\downarrow(k) \\ W_{k+1} &= (-\Delta\tau U)^{k+1} \det D_\uparrow(k+1) \det D_\downarrow(k+1) \end{aligned} \tag{59}$$

If we let the probability to add and remove a vertex be P_a and P_r respectively, (these numbers determine the probability that we call the subroutine which tries to add or subtract a vertex, and $P_a + P_r = 1$), then the detailed balance condition requires that

$$P_a \frac{1}{L}\frac{1}{N} W_k P_{k\to k+1} = P_r \frac{1}{k+1} W_{k+1} P_{k+1\to k} \tag{60}$$

Here $\frac{1}{L}\frac{1}{N}$ is the probability to choose a position in time and space for the vertex you intend to add while $\frac{1}{k+1}$ is the probability to choose one vertex you intend to remove of from the existing $k+1$ ones. If we accept or reject this change using a Metropolis algorithm [11], then we need the Metropolis ratio R.

Suppose we propose to add vertex, then

$$R = P_{k\to k+1}/P_{k+1\to k} = -\frac{U\beta N}{k+1} \prod_\sigma \det D_\sigma(k+1) / \prod_\sigma \det D_\sigma(k) \tag{61}$$

We need an efficient way to calculate the ratio of determinants

$$\begin{aligned} \det D_\sigma(k+1)/\det D_\sigma(k) &= \det D_\sigma(k+1) M_\sigma(k) \\ &= \det\left(I + (D_\sigma(k+1) - D_\sigma(k)) M_\sigma(k)\right) \end{aligned} \tag{62}$$

where $M_\sigma(k) = D_\sigma(k)^{-1}$, and we must pad the matrices $M_\sigma(k)$ and $D_\sigma(k)$ with an extra row and column in the $k+1$ location with all zeroes, except for a 1 in the $k+1$, $k+1$ location.

$$\det\left(I + (D_\sigma(k+1) - D_\sigma(k))M_\sigma(k)\right) = \det \tag{63}$$
$$\begin{pmatrix} 1 & 0 & \cdots & G^0_\sigma(1,k+1) \\ 0 & 1 & \cdots & G^0_\sigma(2,k+1) \\ 0 & 0 & \cdots & G^0_\sigma(3,k+1) \\ . & . & . & \\ . & . & . & . \\ . & . & . & . \\ G^0_\sigma(k+1,i)M(k)_{i,1} & G^0_\sigma(k+1,i)M(k)_{i,2} & \cdots & G^0_\sigma(k+1,k+1) \end{pmatrix}$$

A cofactor expansion (first on the last column and then on the last row) yields

$$\det D_\sigma(k+1)/\det D_\sigma(k) = G^0_\sigma(k+1,k+1) - G^0_\sigma(k+1,i)M(k)_{ij}G^0_\sigma(j,k+1) \tag{64}$$

with an implied sum over repeated indices. Clearly, the matrices M are important for the update, and they, not D are stored. The change is accepted if R is greater than a random number between zero and one. Then, we need an equation used to update M which may be derived using the Inversion by Partitioning described in Numerical Recipes [7].

$$M_\sigma(k+1) = \begin{pmatrix} . & . & . & -\lambda^{-1}L_{1k+1} \\ . & . & . & -\lambda^{-1}L_{2k+1} \\ . & M_\sigma{}' & . & -\lambda^{-1}L_{3k+1} \\ . & . & . & \\ . & . & . & . \\ -\lambda^{-1}R_{k+1,1} & -\lambda^{-1}R_{k+1,2} & \cdots & -\lambda^{-1} \end{pmatrix} \tag{65}$$

where the first k by k section is filled by the matrix

$$M_\sigma{}'_{ij} = M(k)_{ij} + L_{ik+1}\lambda^{-1}R_{k+1,j} \tag{66}$$

and

$$R_{ij} = G^0_\sigma(i,n)M(k)_{nj} \;\; L_{ij} = M(k)_{in}G^0_\sigma(n,j) \tag{67}$$

and λ is given by Eq. 64.

If we propose to remove vertex at location n, then to determine whether to accept the move, we need

$$\det D_\sigma(k-1)/\det D_\sigma(k) = \det\left((M_\sigma(k) - M_\sigma(k-1))D_\sigma(k-1) + I\right) \tag{68}$$

Again, using a cofactor expansion, it is easy to show that this is just $M_{\sigma nn}$. Then if

$$R = \frac{-k}{U\beta N}\prod_\sigma \det D_\sigma(k-1)/\prod_\sigma \det D_\sigma(k) \tag{69}$$

is greater than a random number between zero and one, we accept the change and must update M_σ using

$$M_{\sigma ij}(k-1) = M_{\sigma ij}(k) - M_{\sigma in}(k) M_{\sigma nj}(k) / M_{\sigma nn}(k) \tag{70}$$

One natural question is to ask whether this QMC is convergent, which would require that the average value of k be finite.

$$\begin{aligned}
\langle k \rangle &= \frac{Z_0}{Z} \sum_0^\infty \frac{(-1)^k}{k!} k \int_0^\beta d\tau_1 \cdots d\tau_k \langle T_\tau H_1(\tau_1) \cdots H_1(\tau_k) \rangle_0 \qquad (71) \\
&= -\frac{Z_0}{Z} \sum_0^\infty \frac{(-1)^k}{k!} k \int_0^\beta d\tau_1 \cdots d\tau_k d\tau \langle T_\tau H_1(\tau_1) \cdots H_1(\tau_k) H_1(\tau) \rangle_0 \\
&= -\int_0^\beta d\tau \langle H_1(\tau) \rangle \\
&= -\beta \langle H_1 \rangle
\end{aligned}$$

where the brackets $\langle\rangle$ denote the average with respect to full interacting Hamiltonian (Eq. 1), which is also the average value of Monte Carlo measurements. The last line in Eq. 72 follows if H_1 is independent of τ. Since $\langle H_1 \rangle$ is extensive, this means that $\langle k \rangle = -\beta N \langle h_1 \rangle$ where h_1 is the average potential energy per site.

As will be described below in Sec. 4.1, the minus sign problem emerges when the Metropolis ratio R is not positive definite. It is easy to see from Eqs. 61 and 69 that when $U < 0$ there is no minus sign problem since the up and down determinants the same and real, so their product is positive. However, the minus sign problem can be severe when $U > 0$ since the sign of the sampling weight will fluctuate as k changes by ± 1. Some tricks can be used to control the sign problem. For example, at half filling where there is particle-hole symmetry, we rewrite the interaction as

$$H_1 = U \sum_i \left(n_{\uparrow i} - \frac{1}{2} \right) \left(n_{\downarrow i} - \frac{1}{2} \right) \tag{72}$$

then the particle-hole transformation $c_{j\downarrow} \rightarrow c^\dagger_{j\downarrow}$ changes the sign of U eliminating the sign problem. Away from half filling, this trick is useless. However, here we introduce an additional Ising-like auxiliary field $s_i = \pm 1$ on each site and rewrite the interaction as:

$$H_1 = \frac{U}{2} \sum_{i,s_i} \left(n_{\uparrow i} - \frac{1}{2} - s_i \alpha \right) \left(n_{\downarrow i} - \frac{1}{2} + s_i \alpha \right) \tag{73}$$

At least in 0 or 1 dimension, the choice $\alpha > 1/2$ eliminates the sign problem. The cost is that the Ising field is now associated with each point in space-time and must be sampled using the QMC algorithm.

Since Wick's theorem applies to the configurations of CTQMC, most measurements are simply accomplished by forming the appropriate Wicks contractions of the Green's function

$$G_\uparrow(i,j) = -\left\langle T_\tau c_\uparrow(i) c^\dagger_\uparrow(j) \right\rangle . \tag{74}$$

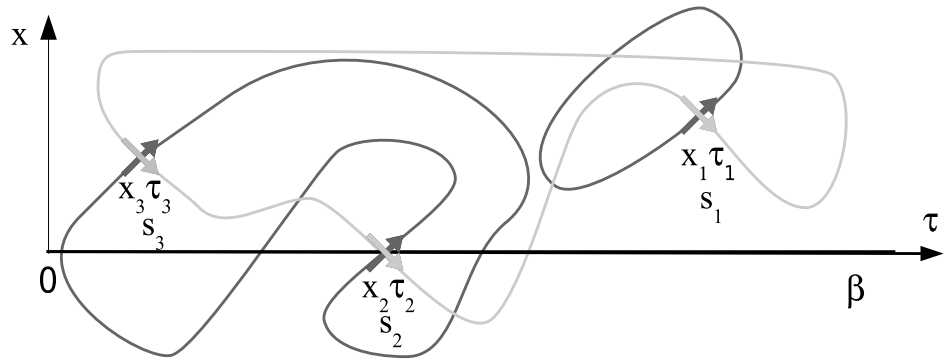

FIGURE 7. An example of a third-order ($k = 3$) CTQMC graph with the Rubtsov auxiliary field used to suppress the minus sign configuration. Now each vertex also carries a field $s_i = \pm 1$ which must be updated along with the vertex locations in the QMC.

corresponding to a configuration of vertices (and auxiliary fields when appropriate).

$$G_\uparrow(i,j) = -\frac{Z_0}{Z}\sum_k \frac{(-U)^k}{k!}\int\cdots\int d1\cdots dk \qquad \left\langle T_\tau c_\uparrow(i)c_\uparrow^\dagger(j)n_\uparrow(1)\cdots n_\uparrow(k)\right\rangle_0 \left\langle T_\tau n_\downarrow(1)\cdots n_\downarrow(k)\right\rangle_0 \tag{75}$$

However, this formula is very similar to the one we encountered when we added a vertex. In fact,

$$G_\uparrow(i,j) = \det D_\uparrow(k+1)/\det D_\uparrow(k) \tag{76}$$

where the $k\times k$ matrix $D_\uparrow(k)$ is given by Eq. 58 and

$$D_\uparrow(k+1) = \begin{pmatrix} G_\uparrow{}^0(1,1) & G_\uparrow{}^0(1,2) & \cdots & G_\uparrow{}^0(1,k) & G_\uparrow{}^0(1,j) \\ G_\uparrow{}^0(2,1) & G_\uparrow{}^0(2,2) & \cdots & G_\uparrow{}^0(2,k) & G_\uparrow{}^0(2,j) \\ G_\uparrow{}^0(3,1) & G_\uparrow{}^0(3,2) & \cdots & G_\uparrow{}^0(3,k) & G_\uparrow{}^0(3,j) \\ \vdots & \vdots & \vdots & \vdots & \\ \vdots & \vdots & \vdots & \vdots & \vdots \\ \vdots & \vdots & \vdots & \vdots & \vdots \\ G_\uparrow{}^0(k,1) & G_\uparrow{}^0(k,2) & \cdots & G_\uparrow{}^0(k,k) & G_\uparrow{}^0(k,j) \\ G_\uparrow{}^0(i,1) & G_\uparrow{}^0(i,2) & \cdots & G_\uparrow{}^0(i,k) & G_\uparrow{}^0(i,j) \end{pmatrix} \tag{77}$$

We obtain the familiar form for

$$G_\uparrow(i,j) = G_\uparrow{}^0(i,j) - G_\uparrow{}^0(i,p)M_{\uparrow pq}G_\uparrow{}^0(q,j)\,. \tag{78}$$

Of course, a similar equation holds for $G_\downarrow$.

All other measurements are then formed from Wick's contractions of these Green's functions, as described in standard many-body texts [6]. This is worth illustrating for one example, such as the transverse component of the spin susceptibility.

$$\chi^\pm(i,j) = -\left\langle T_\tau c_\uparrow^\dagger(i)c_\downarrow(i)c_\downarrow^\dagger(j)c_\uparrow(j)\right\rangle \tag{79}$$

The form for this is strikingly similar to what we did above for $G_\uparrow(i,j)$, the main difference being that we now have both spin components

$$\chi^{\pm}(i,j) = \frac{Z_0}{Z}\sum_k \frac{(-U)^k}{k!}\int d1\cdots dk \qquad \left\langle T_\tau c_\uparrow^\dagger(i)c_\uparrow(j)n_\uparrow(1)\cdots n_\uparrow(k)\right\rangle_0 \left\langle T_\tau c_\downarrow^\dagger(j)c_\downarrow(i)n_\downarrow(1)\cdots n_\downarrow(k)\right\rangle_0 \tag{80}$$

So the estimator is

$$\chi^{\pm}(i,j) = \left\langle \left(G_\uparrow{}^0(j,i) - G_\uparrow{}^0(j,p)M_{\uparrow\,pq}G_\uparrow{}^0(q,i)\right) \left(G_\downarrow{}^0(i,j) - G_\downarrow{}^0(i,p)M_{\downarrow\,pq}G_\downarrow{}^0(q,j)\right)\right\rangle_{QMC} \tag{81}$$

Similar estimators may be formed from $G_\uparrow(i,j)$ and $G_\downarrow(i,j)$ for the longitudinal spin and pair susceptibilities. These will be discussed below.

In order to initialize the QMC process, the number of vertices can be simply set to zero. Subsequent Monte Carlo steps will tend to add vertices until the configuration is thermalized. Alternatively, one can take any other k vertex configuration and use $\mathscr{G}_\sigma$ to construct the D_σ matrices (which are then inverted to obtain M_σ matrices). Here, $\mathscr{G}_\sigma$ is the noninteracting Green's function (i.e. the one obtained when $U=0$) if we mean to simulate a finite size cluster, or its the cluster excluded Green's function (i.e. the one obtained when we subtract the self energy from the cluster) if we mean to simulate an embedded cluster.

Numerical round-off errors accumulate in the M_σ matrices during the updating process, Eqs.66 and 70. In order to eliminate them, after a certain number of iterations they should be refreshed. This may be done by recalculating the D_σ matrices and inverting for the M_σ.

3.1. Combining CTQMC with Quantum Cluster Methods

Quantum cluster methods generally require the Green's function in terms of Matsubara frequency and wavevector, $G(k,i\omega_n)$. However, unlike HFQMC, there is no difficulty in performing the Fourier transform in CTQMC. In fact, this measurement may be made efficiently directly in terms of Matsubara frequency and wavevector, simply by performing a double Fourier transform of the Green's function estimator in Eq. 78

$$G_\uparrow(K_i) = G_\uparrow{}^0(K_i) - G_\uparrow{}^0(K_i)M_\uparrow(K_i)G_\uparrow{}^0(K_i)\,. \tag{82}$$

where now $K=(\mathbf{K},i\omega_n)$ is a frequency-wavevector label, and $M_\uparrow$ is

$$M_\uparrow(K_i) = M_\uparrow(\mathbf{K},i\omega_n) = \sum_{i,j}\exp\left(i\mathbf{K}\cdot(\mathbf{X}_i-\mathbf{X}_j) - i\omega_n(\tau_i-\tau_j)\right)M_{\uparrow\,ij} \tag{83}$$

where i and j label the space-time locations of the vertices.

4. MAKING AND CONDITIONING MEASUREMENTS

The natural byproduct of the QMC algorithm are the Green's functions. These may be used to make measurements of most one and two-particle properties using standard diagrammatic techniques. In doing so, several points must be remembered:

- In the HF QMC algorithm, the Hubbard-Stratonovich transformation reduces the problem to one of free electrons moving in a time-dependent Hubbard-Stratonovich field. In the CTQMC, an interaction representation together with an S-matrix expansion is used. Thus, for each field configuration in the HFQMC or any vertex configuration in the CTQMC, measurements may be formed by summing all allowed Wick's contractions. The full interacting quantity is recovered by QMC averaging this over all configurations.
- It is important to use *all* allowed Wick's contractions, both connected and disconnected, in this series.
- If your Hamiltonian is invariant under translations in space and time, and you are performing a simulation in an unbroken symmetry phase, it is important to average your measurement over all time and space differences in order to achieve the lowest variance estimator..
- It is also important to average over other symmetries of the Hamiltonian, which may not be preserved by the CTQMC or HFQMC algorithms (e.g. spin symmetry).

For example, consider the local impurity magnetic correlation function

$$\begin{aligned}\chi_{ii}(\tau) &\approx \left\langle S_i^+(\tau)S_i^-(0)\right\rangle \\ &\approx \left\langle C_{i\uparrow}^\dagger(\tau)C_{i\downarrow}(\tau)C_{i\downarrow}^\dagger(0)C_{i\uparrow}(0)\right\rangle \\ &\approx \frac{T}{2N}\sum_{i\sigma}\int_0^\beta d\tau' \left\langle G_\sigma(x_i,\tau+\tau';x_i\tau')G_{-\sigma}(x_i\tau';x_i\tau+\tau')\right\rangle_{QMC}\end{aligned} \tag{84}$$

where the *QMC* subscript means that the Monte Carlo average over the Hubbard-Stratonovich fields or vertex configurations is still to be performed. Note that in the last step in Eq. 85 we form all allowed Wick's contractions and average over all equivalent time differences, spins, and sites to reduce the variance of this estimator.

At this point the measurements for CTQMC and HFQMC differ. For CTQMC we essentially have a continuum of Matsubara time, so the time integral in Eq. 85 may be completed very accurately. However, in HFQMC care must be used to reduce the time-step error. Due to time translational invariance, the integral over τ' is not terribly sensitive to $\Delta\tau$ error, so we approximate as a sum using a rectangular approximation. For $\tau > 0$

$$\chi(\tau_l) \approx \frac{1}{2L}\sum_{\sigma,l'}\left\langle G_\sigma(i,ind(l+l');i,l')G_{-\sigma}(i,l';i,ind(l+l'))\right\rangle_{QMC}, \tag{85}$$

where $ind(l)$ is the smaller nonnegative value of either l or $l-L$. For $\tau = 0$ the fact that in HFQMC we always store $G_\sigma(l',l') = G_\sigma(\tau_{l'}+0^+,\tau_{l'})$ requires us to modify the

measurement

$$\chi(\tau=0) \approx \frac{1}{2L}\sum_{\sigma,l'}\left\langle G_\sigma(l',l')\left(G_{-\sigma}(l',l')-1\right)\right\rangle_{QMC}. \tag{86}$$

Finally the susceptibility may be calculated by

$$\chi(T) = \int_0^\beta d\tau\chi(\tau) \approx \sum_l sf(l)\Delta\tau\chi(\tau_l), \tag{87}$$

where the Simpson factor $sf(l) = 2\Delta\tau/3$ ($4\Delta\tau/3$) for odd (even) l is used to reduce the systematic error of the integral.

As a final example, consider the cluster particle-particle Green's function matrix $\chi_c(q,K,K')$ ($K=(\mathbf{K},i\omega_n)$) which in the cluster space-time takes the form

$$\chi_c(X_1,X_2,X_3,X_4) = \left\langle T_\tau c_\uparrow(X_1)c_\downarrow(X_2)c_\downarrow^\dagger(X_3)c_\uparrow^\dagger(X_4)\right\rangle. \tag{88}$$

Here X_i is in the space-(imaginary)time notation $X_i=(\mathbf{X}_i,\tau_i)$, where the points $\mathbf{X}_i$ are on the corresponding reciprocal cluster of $\mathbf{K}$ in real space.

Since the storage associated with this quantity is quite large, it cannot be measured for many times. Thus the measurement in CTQMC and HFQMC are quite similar. First, using Wick's theorem, its value is tabulated for each field configuration and then transformed into the cluster Fourier space. Second, we Monte Carlo average over these configurations. After the first step, the expression for the above two-particle Green's function in the cluster momentum-frequency space becomes

$$\begin{aligned}\chi_c(\mathbf{Q},in_\uparrow{}_n;\mathbf{K},i\omega_n;\mathbf{K}',i\omega_{n'}) &= \Bigg\langle \sum_{X_1,X_4} e^{iK'X_1}G_{c\uparrow}(X_1,X_4)e^{-iKX_4} \\ &\quad \sum_{X_2,X_3} e^{i(Q-K')X_2}G_{c\downarrow}(X_2,X_3)e^{-i(Q-K)X_3}\Bigg\rangle_{QMC}. \end{aligned}\tag{89}$$

where K is the momentum-frequency point $K=(\mathbf{K},i\omega_n)$.

The measurements of $G_{c\uparrow}$ and $G_{c\downarrow}$. However, the sums (integrals) over τ in Eq. 89 require special consideration. Since the Green's functions change discontinuously when the two time arguments intersect, the best applicable integral approximation is the trapezoidal approximation. Using this, we will run into Green's functions $G_c(\mathbf{X},\tau;\mathbf{X},\tau)$ with both time and space arguments the same. In the HFQMC algorithm, this is stored as $G_c(\mathbf{X},\tau^+;\mathbf{X},\tau)$ (i.e. it is assumed that the first time argument is slightly greater than the second) and in CTQMC, the other time ordering is assumed; however, if we replaced the equal time Green's function to be the average $\{G_c(\mathbf{X},\tau^+;\mathbf{X},\tau)+G_c(\mathbf{X},\tau;\mathbf{X},\tau^+)\}/2 = G_c(\mathbf{X},\tau^+;\mathbf{X},\tau)-1/2 = G_c(\mathbf{X},\tau^-;\mathbf{X},\tau+)+1/2$ then a trapezoidal approximation of the integrals results. If we call the matrix $\mathbf{G}_c$, with $1/2$ subtracted (added) from its diagonal elements as appropriate for HFQMC (CTQMC), as $\hat{\mathbf{G}}_c$ (note that we can treat one of the three independent momenta involved in χ_c as a variable Q outside the matrix structure),

then we can write the two-particle Green's function in a matrix form

$$\chi_{c\imath j}(\mathbf{Q}) = \left\langle \left(\mathbf{F}^{\dagger}_{\mathbf{Q}=0}\hat{\mathbf{G}}_{c\uparrow}\mathbf{F}_{\mathbf{Q}=0}\right)_{\imath j}\left(\mathbf{F}^{\dagger}_{\mathbf{Q}}\hat{\mathbf{G}}_{c\downarrow}\mathbf{F}_{\mathbf{Q}}\right)^{*}_{\imath j}\right\rangle_{QMC}, \tag{90}$$

where $(\mathbf{F}_{\mathbf{Q}})_{ij} = \Delta\tau e^{-i(\mathbf{K}_j-\mathbf{Q})\cdot\mathbf{X}_i - i\omega_j\tau_i}$ where we have chosen $\imath$ and j to index the cluster momentum-frequency space.

This measurement may be performed efficiently if the product of three matrices in each set of parenthesis is tabulated as two sequential matrix-matrix products and stored before the direct product between the terms in parenthesis is calculated. When done this way, the calculation time required for this process scales like $(NL)^3$ rather than $(NL)^4$ as would result from a straight-forward evaluation of the sums implicit in Eq. 90. Greater efficiency can be obtained if we perform the Fourier transforms as a two-step process; i.e. first doing the transform in time and then in space. Then the measurement scales like $(N+L)(NL)^2$, of course, these reductions in FLOPs require an increase in memory needed to store the intermediate results.

CTQMC presents the possibility of measuring these two-particle susceptibilities directly in the cluster momentum-frequency space without the need to perform the discrete Fourier transform in Matsubara time presented in Eq. 89. Again, this measurement may be made efficiently again performing a double Fourier transform of the Green's function estimator Eq. 78

$$G_{\uparrow}(K_i,K_j) = {G_{\uparrow}}^0(K_i)\delta_{ij} - {G_{\uparrow}}^0(K_i)M_{\uparrow}(K_i,K_j){G_{\uparrow}}^0(K_j). \tag{91}$$

and $M_{\uparrow}$ is

$$\begin{aligned} M_{\uparrow}(K_n,K_m) &= M_{\uparrow}(\mathbf{K}_n,i\omega_n;\mathbf{K}_m,i\omega_m;) \\ &= \sum_{i,j}\exp\left(i\mathbf{K}_n\cdot\mathbf{X}_i - i\omega_n\tau_i)\right)M_{\uparrow\,ij}\exp\left(-i\mathbf{K}_m\cdot\mathbf{X}_j + i\omega_m\tau_j)\right) \end{aligned} \tag{92}$$

where i and j label the space-time locations of the vertices. The last step is the numerical bottleneck. However,using the methods described above of performing the Fourier transforming steps and storing the intermediate result, this step may be performed in $\mathcal{O}2(L+N)k^2)$ FLOPs. The estimator of the cluster particle-particle then becomes

$$\chi_c(Q,K,K') = \left\langle G_{\uparrow}(K'+Q,K+Q)G_{\downarrow}(-K',-K)\right\rangle_{QMC}. \tag{93}$$

4.1. The minus sign problem

The minus sign problem emerges when the metropolis ratio R is not positive definite. In this case, it can no longer be interpreted as a ratio of probabilities, and the algorithm, as presently described, fails. To deal with this problem, we associate the sign S of each configuration $\{s_i\}$ with the measurement m and not the sampling weight W. That is

$$\langle m\rangle = \frac{\sum_{\{s_i\}} m(\{s_i\})W(\{s_i\})}{\sum_{\{s_i\}} W(\{s_i\})} \tag{94}$$

$$
\begin{aligned}
&= \frac{\sum_{\{s_i\}} m(\{s_i\}) S(\{s_i\}) |W(\{s_i\})|}{\sum_{\{s_i\}} S(\{s_i\}) |W(\{s_i\})|} \\
&= \frac{\sum_{\{s_i\}} m(\{s_i\}) S(\{s_i\}) |W(\{s_i\})| / \sum_{\{s_i\}} |W(\{s_i\})|}{\sum_{\{s_i\}} S(\{s_i\}) |W(\{s_i\})| / \sum_{\{s_i\}} |W(\{s_i\})|} \\
&= \langle mS \rangle_{|W|} / \langle S \rangle_{|W|} \qquad (95)
\end{aligned}
$$

So we may use the absolute value of $|W|$ as the sampling weight as long as we measure the product of the sign and measurement and divide by the average sign. This method will work as long as the average sign is reasonably large, but when $\langle S \rangle_{|W|}$ becomes small, the measurement becomes undefined.

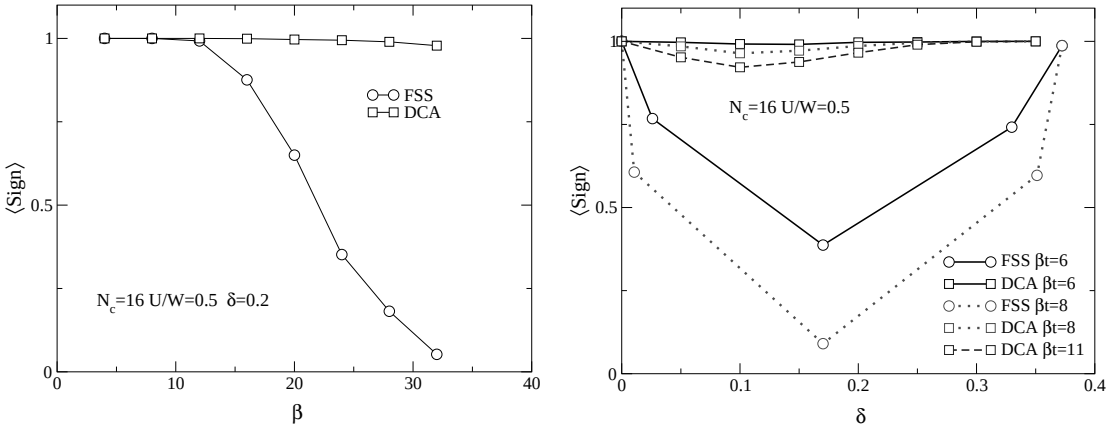

FIGURE 8. Comparison of the average sign from a HFQMC DCA and finite-size simulation (FSS) of the 2D Hubbard model when $N = 16$, $U = 4t = W/2$ versus temperature (left) and filling (right).[4]

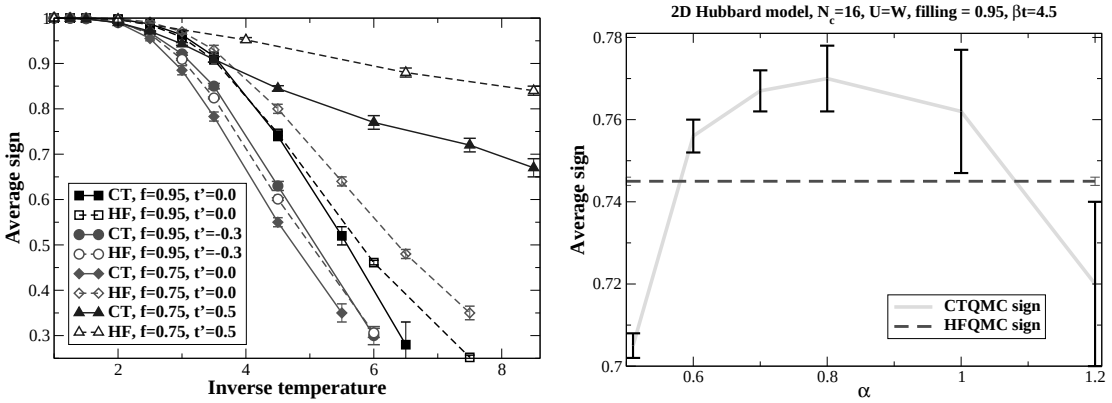

FIGURE 9. Comparison of the average sign from a CTQMC and HFQMC DCA simulation of the two-dimensional Hubbard model. (Left) Average sign versus inverse temperature for 4-site cluster with $U = W = 8t$ and different fillings. (Right) the average sign for 16-site cluster with $U = W = 8t$ versus α from Eq. 73 at fixed filling and temperature.

The average sign obtained from a simulation of the 2D Hubbard model is shown in Fig. 9. The average sign from HFQMC and CTQMC are similar but the CTQMC result is slightly worse. The figure on the right shows that increasing the value of α from Eq. 73 does not help to increase the average sign significantly and it also increases the

error bar on the sign measurement due to an increase in the average order $\langle k \rangle$. The error bar increases, since the average order $\langle k \rangle$ increases like α^2 for large α as may be seen from Eq. 72, or here (for some site i).

$$\begin{aligned} \langle k \rangle &= -\beta \langle H_1 \rangle \\ &= -N\beta \left\langle \sum_{s_i} \left(n_{\uparrow i} - \frac{1}{2} - s_i \alpha \right) \left(n_{\downarrow i} - \frac{1}{2} + s_i \alpha \right) \right\rangle \end{aligned} \tag{96}$$

On the other hand, the average sign obtained from a simulation of the 1D Hubbard model is shown in Fig. 10. Whereas the average sign from HFQMC depends weakly with cluster size that from CTQMC actually *increases* strongly with increasing cluster size. Also studied is an additional coupling between chains t_{perp}/t which is a hopping between equivalent sites on adjacent chains. A finite t_{perp}/t causes the average sign to increase strongly.

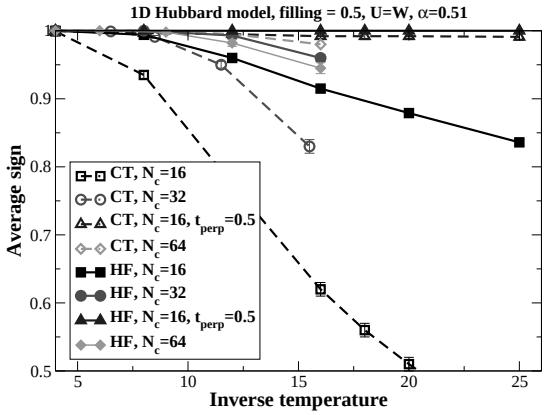

FIGURE 10. Comparison of the average sign from a CTQMC and HFQMC DCA simulation of the one-dimensional Hubbard model. The average sign of HFQMC depends weakly on the cluster size; whereas the average sign of CTQMC increases strongly with increasing cluster size.

We find that the average sign depends on many things, fillings, dimensionality model parameters, etc. It is difficult to predict *a priori* whether the average sign will be problematic.

4.2. CTQMC and real time measurements

In this section, we briefly discuss a possibility to extend CTQMC to measure real time Green's functions or even treat the systems out of thermal equilibrium. We start with the same Hubbard model Hamiltonian [2], which has no time dependent terms, and proceed to derive expressions for partition function and real time Green's functions. In this formalism, the partition function can be expressed as an expansion of contour ordered exponent:

$$Z = Z_0 \sum_{k=0}^{\infty} \frac{(-i)^k}{k!} \int_c dt_1 \ldots \int_c dt_k \, \langle T_c H_1(t_1) \ldots H_1(t_k) \rangle_0 \tag{97}$$

where

$$H_1(t) = e^{iH_0 t} H_1 e^{-iH_0 t} \tag{98}$$

is the interaction (quartic) part of Hamiltonian in the interaction representation and T_c

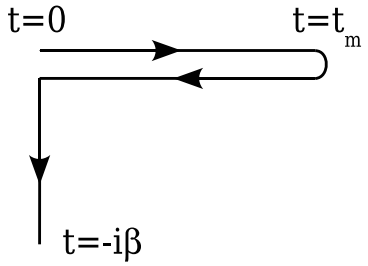

FIGURE 11. The contour for measuring the real time Green's function.

is the contour-ordering operator. The integrals are performed along the contour c, shown in Fig. 11. By writing out the contributions to the partition function coming from lowest orders in expansion (Eq. 97), one can see that all the terms containing $H_1(t)$ on real parts of contour cancel out exactly and thus the partition function in this case is the same as in Matsubara formalism. We now consider the expansion for the contour ordered Green's function:

$$\begin{aligned} G_c(t,t') &= \left\langle T_c c(t) c^\dagger(t') \right\rangle \\ &= -i\frac{Z_0}{Z} \sum_{k=0}^{\infty} \frac{(-i)^k}{k!} \int_c dt_1 \ldots \int_c dt_k \left\langle T_c c(t) c^\dagger(t') H_1(t_1) \ldots H_1(t_k) \right\rangle_0 \end{aligned} \tag{99}$$

In this case, however, the contributions containing $H_1(t)$ on real parts of contour do not cancel out (as one can easily check by writing out $k = 1$ term in the expansion). The application of Wick's theorem yields CTQMC diagrams that contain vertices on both imaginary as well as real parts of contour (See Fig. 12). Thus, the partition function and the Green's function have dominant contributions coming from entirely different regions in the k-dimensional space spanned by time coordinates along the contour. As a consequence, it appears impossible to use the partition function as a sampling weight in Monte Carlo algorithm to measure the Green's function. It is still possible to use the

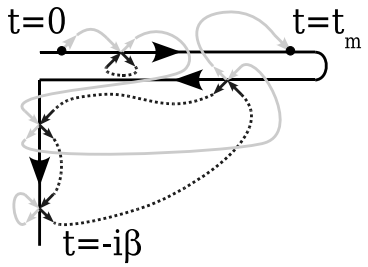

FIGURE 12. An example ($k = 4$) diagram for contour ordered Green's function for spin up electrons. The light continuous and darker dotted lines represent the propagators for spin up and spin down electrons, respectively.

Green's function itself as a weight in the Monte Carlo importance sampling, and then

measure it's value as a distribution in the space of it's arguments (t,t'). Since Green's function in this case would be a complex number, it's modulus would be taken for the sampling weight instead. The sign problem would now translate into the phase problem, if the average value of the phase of the Green's function gets too small. By looking at Eq. 100 we see that the phase problem is likely to be very severe due to a factor of $(-i)$ attached to every vertex on the real part of the contour (unless one finds again a way to introduce an auxiliary field that remedies this problem). In any case, the oscillatory nature of real time Green's function implies that the phase problem would most likely restrict measurements of Green's function to small values of its real time arguments.

5. CONCLUSION

We would like to acknowledge useful conversations and fruitful collaborations with J. K. Freericks, B. Goodman, E. Gull, M. Hettler, H. R. Krishnamurthy, M. Ma, Th. Maier, Th. Pruschke, R. Scalettar, M. Troyer, and F. C. Zhang. This work was supported by the National Science Foundation grants DMR-0706379 and DMR-0312680.

REFERENCES

1. J. Hubbard, Proc. R. Soc. A **276**, 238 (1963); M.C. Gutzwiller, Phys. Rev. Lett. **10**, 159 (1963); J. Kanamori, Prog. Theor. Phys. **30**, 257 (1963).
2. J.E. Hirsch and R.M. Fye, Phys. Rev. Lett. **56**, 2521 (1986).
3. R.M. Fye and J.E. Hirsch, Phys. Rev. B **38**, 433 (1988).
4. M. Jarrell, Th. Maier, C. Huscroft, and S. Moukouri, Phys. Rev. B **64**, 195130/1-23 (2001).
5. J.E. Hirsch, Phys. Rev. B, **28**, 4059 (1983), and **31**, 4403 (1985).
6. A.A. Abrikosov, L.P. Gorkov, I.E. Dzyalishinski, *Methods of Quantum Field Theory in Statistical Physics*, (Dover, New York, 1975).
7. William H. Press, Saul A. Teukolsky, William T. Vetterling, and Brian P. Flannery, *Numerical Recipes in Fortran 77*, Second Edition (1992), Cambridge University Press.
8. M. Jarrell, H. Akhlaghpour, and Thomas Pruschke, **Quantum Monte Carlo Methods in Condensed Matter Physics**, Ed. M. Suzuki, (World Scientific, 1993).
9. Transactions on Mathematical Software, Vol. **22**, No. 3, p. 362–371 (September, 1996).
10. A. N. Rubtsov, V. V. Savkin, A. I. Lichtenstein, Phys. Rev. B **72**, 035122 (2005)
11. N. Metropolis, A. W. Rosenbluth, M. N. Rosenbluth. A. H. Teller and E. Teller, J. Chem. Phys. **21**, 1087-1092 (1953).